Journal of Electroanalytical Chemistry, **839**, 173-176 (2019).

Improved electrochemical performances in a bismuth fluoride electrode prepared using a high energy ball mill with carbon for fluoride shuttle batteries

Hiroaki Konishi,[a, z] Asuman Celik Kucuk,[b] Taketoshi Minato,[b, z] Takeshi Abe,[c, z] and Zempachi Ogumi,[a]

[a] Office of Society-Academia Collaboration for Innovation, Kyoto University, Gokasho, Uji, Kyoto 611-0011, Japan

[b] Office of Society-Academia Collaboration for Innovation, Kyoto University, Katsura, Nishikyo, Kyoto 615-8510, Japan

[c] Graduate School of Global Environmental Studies, Kyoto University, Katsura, Nishikyo, Kyoto 615-8510, Japan

[z] **Corresponding author**

Hiroaki Konishi

E-mail: hiroaki.konishi.yj@hitachi.com

Taketoshi Minato

E-mail: minato.taketoshi.5x@kyoto-u.ac.jp

Takeshi Abe

E-mail: abe@elech.kuic.kyoto-u.ac.jp

Present address

Hiroaki Konishi

Research & Development Group, Hitachi Ltd.

Hitachi, Ibaraki 319-1292, Japan

E-mail: hiroaki.konishi.yj@hitachi.com

Keywords

anion acceptor; ball mill; bismuth fluoride; fluoride shuttle battery

Abstract

Bismuth fluoride (BiF_3) is a promising positive electrode material for fluoride shuttle batteries (FSBs) owing to its high theoretical specific capacity (302 mA h g^{-1}). However, it exhibits low practical capacity. The methods for preparing the electrode are known to have significant effects on battery performance. The mixture between BiF_3 and carbon, BiF_3/C, prepared by high energy ball milling method has been already approved in lithium ion batteries. With this method, a significant improvement over the discharge and charge capacities of the BiF_3/C electrode has been achieved. In this work, for the first time, BiF_3/C electrode has been used for FSB. Using BiF_3/C electrode significantly increased the discharge and charge capacities. To confirm the progress of the discharge and charge reactions of BiF_3/C electrode, the crystal structure of active materials and oxidation state of Bi for the BiF_3/C electrode during discharge and charging has been investigated by X-ray diffraction and X-ray absorption fine structure. The results reveal that, with higher capacity values, discharge and charge reactions related to BiF_3/C have been realized.

Introduction

Lithium-ion batteries (LIBs) have been widely used in a lot of portable electronic devices such as laptop computers and smartphones [1–3]. Regarding the incredible advances in technology, high-energy-density batteries that surpass the performance of LIBs are inevitably required in new future. Therefore, many research groups have been focusing on developing next-generation batteries [4–8]. A battery utilizing fluoride ion migration in electrochemical reactions that has recently introduced may have potential to meet expectations [9–18]. In this battery, metal fluoride (MF_x, M: metal) is used as a positive electrode material, and its electrochemical reaction progresses according to the following formulae:

Discharge process: $MF_x + xe^- \rightarrow M + xF^-$

Charge process: $M + xF^- \rightarrow MF_x + xe^-$

Recently our group reported some studies based on FSB operated at the room temperature [19–22]. In these studies, the inorganic fluoride compound was dissolved in an organic solvent using an anion acceptor (AA) for the first time, and the electrochemical behavior of BiF_3 electrode in the electrolyte comprising organic solvent (bis[2-(2-methoxyethoxy)ethyl] ether (tetraglyme: G4)), supporting electrolyte salt (cesium fluoride (CsF)), and AA (fluorobis(2,4,6-trimethylphenyl)borane (FBTMPhB)). In the first experiment, to ensure complete dissolution of CsF, AA was used at higher

concentration than CsF [19]. On the other hand, in the subsequent experiment, the concentration of AA was kept the same while CsF concentration was increased to saturation level, and it has been found that higher concentration of CsF compare to AA has positive impact on the cycling performance of BiF_3; however, its reversible capacity value has been found to be still less than the theoretical specific capacity (302 mAh g^{-1}) [20]. The BiF_3 has been recently investigated as an active material in LIB since it exhibits high theoretical specific capacity; however, its practical capacity was much less than the theoretical capacity due to low electronic conductivity [23, 24]. To overcome this problem, BiF_3 has been blended with carbon by high energy ball milling method, and a significant capacity improvement has been obtained in LIB [23–33]. This success greatly motivates us to use this process with the FSB system we have already developed.

In this research, non-treated BiF_3 and BiF_3 blended with carbon using a planetary ball mill were prepared. Their discharge and charge capacities were evaluated in the G4 containing 0.5 mol dm^{-3} FBTMPhB and saturated CsF, and the effect of the blend with carbon on the electrochemical performances were investigated. The progression on the related discharge and charge reactions were confirmed using X-ray diffraction (XRD) and X-ray absorption fine structure (XAFS).

2. Experimental

The BiF_3 (Fluorochem Ltd.) was pulverized for 1 h in a planetary ball mill (FRITSCH

PULVERISETTE 7) at 1100 rpm. Next, 80 wt% of pulverized BiF_3 and 20 wt% of acetylene black (AB) were mixed for 1 h in a planetary ball mill at 1100 rpm; the resulting material was referred to BiF_3/C. The samples were sealed in the planetary ball mill under argon atmosphere. The BiF_3 and BiF_3/C were used as the active material. The particle configuration of the BiF_3 and BiF_3/C powders was observed using scanning electron microscopy (SEM; Hitachi SU6600). The energy of the incident electrons was 20 keV.

The electrochemical performances of prepared samples were evaluated as follows. First, the electrolyte for FSB was prepared by adding 0.5 mol dm^{-3} CsF (Tokyo Chemical Industry Co., Ltd) and 0.5 mol dm^{-3} FBTMPhB (Tokyo Chemical Industry Co., Ltd) to G4 (Kishida Chemical Co., Ltd). After addition of these compounds to G4, it was found that CsF partly remained undissolved in G4. Its supernatant solution was used as the electrolyte. The electrolyte was prepared in a glove box filled with high-purity argon. Second, the electrodes were prepared by following method. The BiF_3 or BiF_3/C, AB, and polyvinylidene difluoride (60:25:15 (BiF_3) or 75:10:15 (BiF_3/C) wt%) were mixed, followed by the addition of N-methyl-2-pyrrolidone (NMP). The resulting slurry was coated on an aluminum current collector, and NMP was removed by heating at 110°C. The discharge and charge capacities of the BiF_3 and BiF_3/C electrodes were measured using a three-electrode electrochemical cell (EC FRONTIER CO., Ltd. VB7) comprising a BiF_3 or BiF_3/C electrode, a platinum mesh, and a silver rod immersed in acetonitrile containing 0.1 mol dm^{-3} of silver nitrate and 0.1 mol dm^{-3} of

tetraethylammonium perchlorate as the working electrode, counter electrode, and reference electrode (0.587 V vs. standard hydrogen electrode) [34], respectively. The electrochemical cell was assembled in a glove box filled with high-purity argon. Charge and discharge measurements were carried out using a multipotentiostat (Biologic VMP-300) at potentials ranging from –2.0 to –0.3 V (vs. ref.) at 0.025C (1C: 302 mA g^{-1}) and at room temperature under argon atmosphere. Specific capacities of BiF_3 and BiF_3/C were obtained by dividing the capacity by the weight of the active material (BiF_3).

The progress of discharge and charge reactions for the BiF_3/C electrode was confirmed by XRD and XAFS. The crystal structure of the active materials and oxidation state of Bi for the BiF_3/C electrode in the pristine state, partially discharged state (–1.6 V), fully discharged state (–2.0 V), partially charged state (–0.9 V), and fully charged state (–0.3 V) was investigated by XRD and XAFS. After the BiF_3/C electrodes were discharged and charged, electrodes were washed with G4, followed by dimethyl carbonate to remove the residual electrolyte. XRD patterns were recorded on a Rigaku Smartlab diffractometer equipped with Cu Kα radiation (λ = 1.54 Å) at 2θ ranging from 25 to 50°. The XAFS spectra were obtained at BL14B2 of the Super Photon ring-8 (SPring-8) in Japan. The oxidation state changes of Bi was mainly evaluated by X-ray absorption near-edge structure (XANES) analysis, which were measured in transmission mode using an Si (111) double-crystal monochromator. The XANES data were analyzed using Athena [35].

3. Results and Discussion

Our aims of the ball milling of BiF_3 with AB is to decrease the particle size of BiF_3 and enhance the contact of BiF_3 with AB. The change of the particle configuration from BiF_3 to BiF_3/C powders were analyzed by SEM observations. The obtained SEM images of BiF_3 and BiF_3/C powders are shown in Fig.1. The observed particle size of BiF_3 in the SEM image was 0.5–2.0 μm (Fig. 1(a)). After the ball milling, the particles of 0.1–0.2 μm were observed in the SEM images of BiF_3/C powder (Fig. 1(b)). Although the particles of BiF_3 and AB could not be distinguished by the SEM image of BiF_3/C powder, the size of all particle in the SEM image of BiF_3/C powder (Fig. 1(b)) is smaller than that of BiF_3 (Fig. 1(a)). The decreasing of the particle size means that the specific surface area is increased by the pulverization. The increase in the specific surface area indicates the increase in the contact area on BiF_3 with AB. Also, the obtained indistinctive feature of BiF_3 and AB in BiF_3/C powder observed by SEM means that the BiF_3 are well mixed with AB. These experimental results indicate that the mixing and pulverization using a planetary ball mill leads to the adhesion of AB on BiF_3 particles as we aimed. The decreasing of the particle size increases the interface between active materials and electrolyte for electrochemical reactions, and adhesion of AB on BiF_3 was effective in forming electronic conductive network in the electrode. These suggest that the prepared BiF_3/C would be better active materials for FSB than BiF_3.

To study the electrochemical performance of BiF_3/C for FSB, the discharge and charge

behaviors of BiF_3 and BiF_3/C electrodes have been investigated (Fig. 2). The discharge/charge capacities in the first cycle of the BiF_3 and BiF_3/C electrodes were 212/95 and 427/239 mAh g^{-1}, respectively. Furthermore, the potential of discharge curve for BiF_3/C electrode was higher than that for BiF_3 electrode, and the potential of charge curve for the former was lower than that for the latter. The decreasing of the particle size of BiF_3 and adhesion of AB on BiF_3 would effectively work to achieve the higher capacity and lower polarization in BiF_3/C electrode. The charge capacities of BiF_3 (95 mAh g^{-1}) and BiF_3/C (239 mAh g^{-1}) were found to be lower than their discharge capacities (212 and 427 mAh g^{-1} for BiF_3 and BiF_3/C, respectively). These indicate that the formation of BiF_3 (charge reaction) progressed less than the formation of Bi (discharge reaction) and/or the decomposition of electrolyte progressed during discharging.

The measurements of discharge and charge behavior clearly showed the ball milling of BiF_3 with AB significantly increases the discharge and charge capacities of BiF_3. To verify the progress of the discharge and charge reactions for the BiF_3/C electrode, the change in the crystal structure of active materials and oxidation state of Bi in the BiF_3/C electrode during discharging and charging were evaluated using XRD and XAFS, respectively. The XRD patterns of BiF_3/C electrode during discharging and charging are shown in Fig. 3. All diffraction peaks observed for BiF_3/C in the pristine state corresponded to the orthorhombic phase, except for that observed at $2\theta = 28°$, which was indexed to the hexagonal phase with the *P*–3*c*1 space group (denoted by white square). From the pristine to

the partially discharged state (–1.6 V), the new peaks that assigned to Bi metal were appeared (denoted by black triangle). From the partially discharged to fully discharged state, the intensity of peaks assigned to BiF_3 decreased, and the intensity of peaks assigned to Bi metal increased, indicating that discharge reaction ($BiF_3 + 3e^- \rightarrow Bi + 3F^-$) progressed. Furthermore, the peaks indexed to Cs were appeared (denoted by asterisk) in the fully discharged state, indicating that the decomposition of electrolyte progressed during discharging. In contrast, from the fully discharged to partially charged followed by fully charged state, the intensity of peaks indexed to Bi metal decreased, and the intensity of peaks indexed to BiF_3 increased. These results indicate that the charge reaction ($Bi + 3F^- \rightarrow BiF_3 + 3e^-$) progressed.

Next, the Bi *K*-edge XANES spectra of BiF_3/C electrode during discharging and charging are shown in Fig. 4. From the pristine to the partially discharged (–1.6 V) followed by fully discharged state (–2.0 V), the spectrum shifted to lower energy side and the shape of spectrum changed. The shape of spectrum in the fully discharged state (–2.0 V) was similar to that of Bi metal [27]. These results indicate that Bi was reduced during discharging. In contrast, from the fully discharged (–2.0 V) to partially charged (–0.9 V) followed by fully charged state (–0.3 V), the spectrum shifted to higher energy side and the shape of spectrum changed. These results indicate that Bi was oxidized during charging. These results support the formation of Bi and BiF_3 during discharging and charging, which was confirmed from the XRD results (Fig. 3).

The above results showed that the discharge and charge reactions progress in BiF_3/C electrode in the first cycle. For rechargeable battery, the cycles of the discharge and charge reactions are required. The cycling performance of BiF_3/C electrode for discharge and charge reactions was evaluated. The obtained discharge and charge curves of BiF_3/C in the first, second, third, fourth, fifth, seventh, and tenth cycles are shown in Fig. 5. The discharge/charge capacities of BiF_3/C electrode in the first, second, third, fourth, fifth, seventh, and tenth cycles were 427/239, 252/207, 207/181, 183/161, 163/148, 145/135, and 132/119 mAh g^{-1}, respectively. Although the discharge and charge capacities of BiF_3/C gradually decreased from the first to the tenth cycle, the discharge and charge reactions clearly progressed in the tenth cycle. The capacity degradation was observed in the BiF_3/C electrode operated in LIB system [24]. For the BiF_3/C electrode, the volume of active material largely changed during discharging and charging. The partial isolation of active material due to large volume change causes the capacity degradation during the cycling [24]. Although the capacity of BiF_3/C electrode was decreased during the cycling, the obtained reversible capacity of BiF_3/C in the tenth cycle is higher than that of BiF_3 in the first cycle (Fig. 2), thus it is concluded that the ball milling of BiF_3 with AB is an effective method to increase the discharge and charge capacities of FSB.

In conclusion, it was observed that the use of a planetary ball mill of BiF_3 with AB led to the decrease in the particle size of BiF_3 and the adhesion of AB on BiF_3. The electrochemical results of prepared BiF_3/C showed significantly increased discharge and charge capacities by the

pulverization and adhesion of AB. Furthermore, repeated discharge and charge reactions were observed with FSB system. It is clarified that the using of a planetary ball mill of active material with AB is useful to improve the battery performance of FSB.

Acknowledgements

This work was supported by the Research and Development Initiative for Scientific Innovation of New Generation Batteries (RISING) and Research and Development Initiative for Scientific Innovation of New Generation Batteries 2 (RISING2) projects from the New Energy and Industrial Technology Development Organization (NEDO), Japan. The authors thank Ms. Kiyomi Ishizawa, Ms. Ryoko Masuda, and Ms. Hisayo Ikeda for their experimental support.

References

[1] Y. Nishi, J. Power Sources 100 (2001) 101–106.

[2] Y. Wang, B. Liu, Q. Li, S. Cartmell, S. Ferrara, Z.D. Deng, J. Xiao, J. Power Sources 286 (2015) 330–345.

[3] T. Minato, T. Abe, Prog. Surf. Sci. 92 (2017) 240–280.

[4]. C. Delmas, J. J. Braconnier, C. Fouassier, and P. Hagenmuller, Solid State Ion. 3–4 (1981) 165–169.

[5] D. Aurbach, Z. Lu, A. Schechter, Y. Gofer, H. Gizbar, R. Turgeman, Y. Cohen, M. Moshkovich, and E. Levi, Nature 407 (2000) 724–727.

[6] K. M. Abraham, and Z. Jiang, J. Electrochem. Soc. 143 (1996) 1–5.

[7] T. B. Kim, J. W. Choi, H. S. Ryu, G. B. Cho, K. W. Kim, J. H. Ahn, K. K. Cho, and H. J. Ahn, J. Power Sources 174 (2007) 1275–1278.

[8] A. Eftekhari, J. Power Sources 126 (2004) 221–228.

[9] M. A. Reddy, M. Fichtner, J. Mater. Chem. 21 (2011) 17059–17062.

[10] C. Rongeat, M. A. Reddy, R. Witter, M. Fichtner, J. Phys. Chem. C 117 (2013) 4943–4950.

[11] F. Gschwind, Z. Zhao-Karger, M. Fichtner, J. Mater. Chem. A 2 (2014) 1214–1218.

[12] C. Rongeat, M. A. Reddy, T. Diemant, R.J. Behm, M. Fichtner, J. Mater. Chem. A 2 (2014) 20861–20872.

[13] F. Gschwind, J. Bastien, J. Mater. Chem. A 3 (2015) 5628–5634.

[14] F. Gschwind, G. Rodriguez-Garcia, D.J.S. Sandbeck, A. Gross, M. Weil, M. Fichtner, N. Hormann, J. Fluorine Chem. 182 (2016) 76–90.

[15] H. Bhatia, D.T. Thieu, A.H. Pohl, V.S,K, Chakravadhanula, M.H. Fawey, C. Kubel, M. Fichtner, ACS Appl. Mater. Interfaces 9 (2017) 23707–23715.

[16] M.A. Nowroozi, K. Wissel, J. Rohrer, A.R. Munnangi, O. Clemens, Chem. Mater. 29 (2017) 3441–3453.

[17] A. Grenier, A.Porras-Gutierrez, H. Groult, K.A. Beyer, O.J. Borkiewicz, K.W. Chapman, D. Dambournet, J. Mater. Chem. A 5 (2017) 15700–15705.

[18] D.T. Thieu, M.H. Fawey, H. Bhatia, T. Diemant, V.S,K, Chakravadhanula, R.J. Behm, C. Kubel, M. Fichtner, Adv. Funct. Mater. 27 (2017) 1701051.

[19] H. Konishi, T. Minato, T. Abe, Z. Ogumi, J. Electrochem. Soc. 164 (2017) A3702–A3708.

[20] H. Konishi, T. Minato, T. Abe, Z. Ogumi, J. Appl. Electrochem. 48 (2018) 1205–1211.

[21] H. Konishi, T. Minato, T. Abe, Z. Ogumi, J. Electrocnal. Chem. Electrochem. 826 (2018) 60–64.

[22] H. Konishi, T. Minato, T. Abe, Z. Ogumi, Chem. Lett. 47 (2018) 1346–1349.

[23] M. Bervas, F. Badway, L. C. Klein, and G. G. Amatucci, Electrochem. Solid-State Lett., 8 (2005) A179–A183.

[24] H. Konishi, T. Minato, T. Abe, and Z. Ogumi, J. Electroanal. Chem. 806 (2017) 82–87.

[25]. M. Bervas, F. Badway, L. C. Klein, and G. G. Amatucci, Electrochem. Solid-State Lett. 8 (2005) A179–A183.

[26] M. Bervas, L. C. Klein, and G. G. Amatucci, J. Electrochem. Soc. 153 (2006) A159−A170.

[27] M. Bervas, A. N. Mansour, W. S. Yoon, J. F. Al-Sharab, F. Badway, F. Cosandey, L. C. Klein, and G. G. Amatucci, J. Electrochem. Soc., 153 (2006) A799–A808.

[28] A.J. Gmitter, F. Badway, S. Rangan, R.A. Bartynski, A. Halajko, N. Pereira, and G.G. Amatucci, J. Mater. Chem., 20 (2010) 4149–4161.

[29] B. Hu, X. Wang, Y. Wang, Q. Wei, Y. Song, H. Shu, X. Yang, J. Power Sources 218 (2018) 204–211.

[30] B. Hu, X. Wang, H. Shu, X. Yang, L. Liu, Y. Song, Q. Wei, H. Hu, H. Wu, L. Jiang, and X. Liu, Electrochim. Acta, 102 (2013) 8–18.

[31] J. K. Ko, A. Halajko, M. F. Parkinson, and G. G. Amatucci, J. Electrochem. Soc. 162 (2015) A149–A154.

[32] H. Konishi, T. Minato, T. Abe, and Z. Ogumi, Chemistry Select 2 (2017) 3504–3510.

[33] H. Konishi, T. Minato, T. Abe, and Z. Ogumi, Chemistry Select 2 (2017) 6399–6406.

[34] V. V. Pavlishchuk, and A. W. Addison, Inorg. Chim. Acta 298 (2000) 97–102.

[35] M. Newville, J. Synchrotron Radiat. 8 (2001) 322–324.

Figures

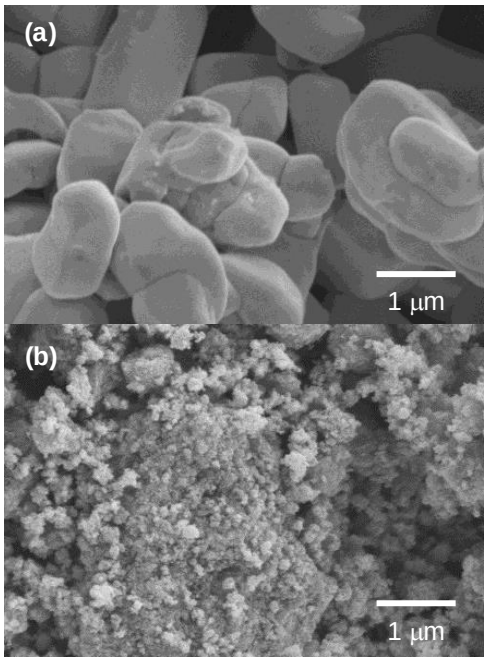

Fig. 1. SEM images of (a) BiF_3 and (b) BiF_3/C powders.

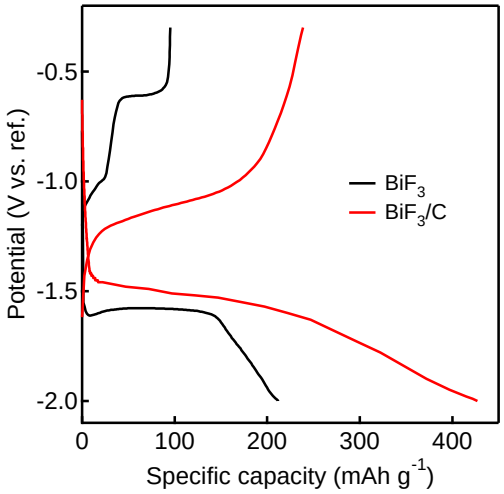

Fig. 2. Discharge and charge curves of BiF_3 and BiF_3/C over the potential range between –2.0 and –0.3 V (vs. ref.) in the first cycle [The data of black line was reproduced from the data of ref. [20]].

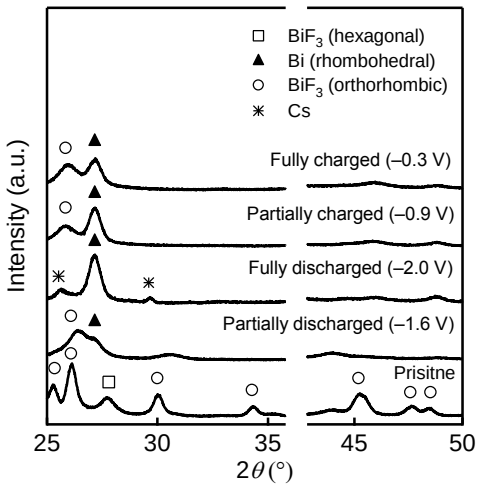

Fig. 3. XRD patterns of BiF_3/C in the pristine, partially discharged (–1.6 V), fully discharged (–2.0 V), partially charged (–0.9 V), and fully charged (–0.3 V) states in the first cycle.

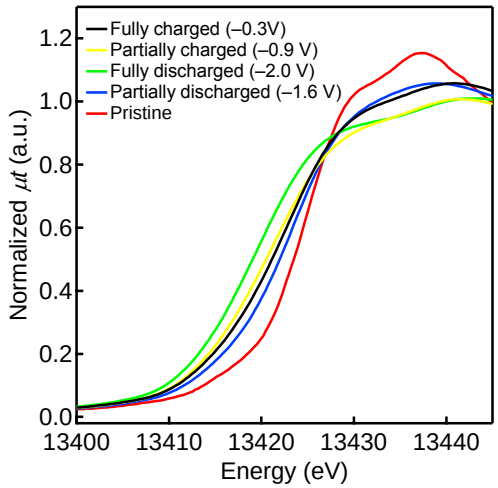

Fig. 4. Bi *K*-edge XANES spectra of BiF_3/C in the pristine, partially discharged (–1.6 V), fully discharged (–2.0 V), partially charged (–0.9 V), and fully charged (–0.3 V) states in the first cycle.

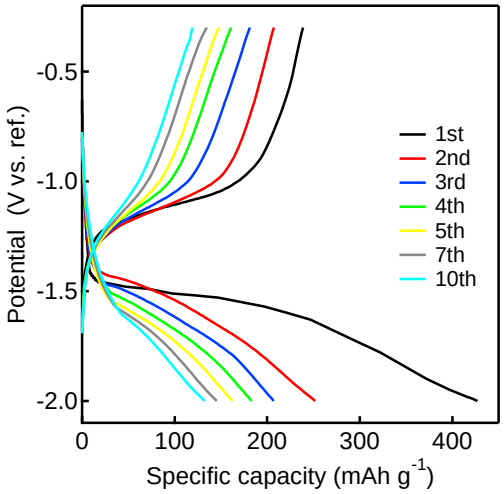

Fig. 5. Discharge and charge curves of BiF_3/C over the potential range between –2.0 and –0.3 V (vs. ref.) in the first, second, third, fourth, fifth, seventh, and tenth cycles.